ACS APPLIED MATERIALS & INTERFACES

Research Article

www.acsami.org

ZnO Nanorods with Low Intrinsic Defects and High Optical Performance Grown by Facile Microwave-Assisted Solution Method

Jie Tang,[†,‡] Jianwei Chai,[§] Jian Huang,[†] Liyuan Deng,[†] Xuan S. Nguyen,[∥] Linfeng Sun,[⊥] T. Venkatesan,[‡] Zexiang Shen,[⊥] Chuan Beng Tay,*[,†,‡] and Soo Jin Chua*[,†,‡,§,∥]

[†]Electrical and Computer Engineering, National University of Singapore, Singapore 117576

[‡]NUSNNI-Nanocore, National University of Singapore, Singapore 117576

[§]Institute of Materials and Research Engineering, Agency for Science, Technology and Research, 3 Research Link, Singapore 117602

[∥]Singapore MIT Alliance Research and Technology, 1 CREATE Way, #10-01 CREATE Tower, National University of Singapore, Singapore 138602

[⊥]Division of Physics and Applied Physics, School of Physical and Mathematical Sciences, Nanyang Technological University, Singapore 637371

Supporting Information

ABSTRACT: Vertically aligned ZnO nanorods were grown at 90 °C by both microwave synthesis and traditional heated water bath method on Si (100) substrate with a precoated ZnO nanoparticle seed layer. A detailed comparison in the morphology, defects, and optical properties of the ZnO nanorods grown by the two methods across the pH range of 10.07−10.9 for microwave synthesis and conventional heated water bath method was performed using scanning electron microscopy, photoluminescence, and X-ray photoelectron spectroscopy. The results show that the microwave route leads to more uniformly distributed nanorods with a lower density of native defects of oxygen interstitials and zinc vacancies. The microwave synthesis presents a promising new approach of fabricating metal oxide nanostructures and devices toward green applications.

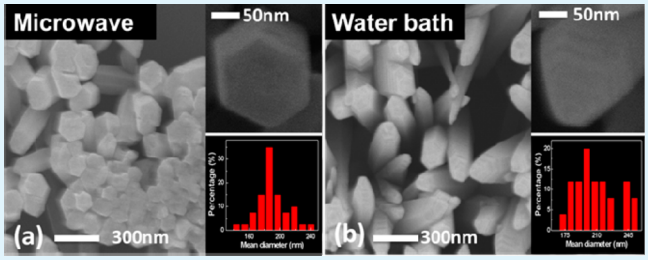

KEYWORDS: *ZnO, microwave synthesis, defects, photoluminescence*

1. INTRODUCTION

Zinc oxide (ZnO) is a fascinating semiconductor with a wide range of properties for multifunctional applications, such as solar cells, varistors, LEDs, nanogenerators, chemical and gas sensors, and spintronic devices, due to its large bandgap (3.37 eV) with high transparency in the visible range, light emitting property with a large exciton binding energy (60 meV), high electrical conductivity, large piezoelectric coefficient, and promising magnetic properties.[1−4] To fully realize the potential of ZnO for these applications, researchers have explored various ZnO growth approaches, including metal organic chemical vapor deposition (MOCVD),[5] pulsed laser deposition (PLD),[6] molecular beam epitaxy (MBE),[7] electrodeposition process,[8] and aqueous solution.[9−11] Among these methods, aqueous solution growth has the advantages of low cost, simple setup, low energy consumption, and a wide variety of easily achievable nanostructures. It has been widely adopted by scientists to fabricate various devices. Nguyen et al. have successfully fabricated a coaxial ZnO nanorods UV LED using solution method.[9] Govender et al. demonstrated an optically pumped broadband visible laser based on ZnO nanowire arrays grown by a wet chemical method.[12] Mahpeykar et al. utilized microwave-assisted hydrothermally synthesized ZnO nanowires for dye-sensitized solar cells.[13] Liu et al. achieved a ZnO nanorod flexible strain sensor and strain driving transistor with an ultrahigh on and off ratio using a single-step hydrothermal reaction.[14]

In comparison to the traditional water bath heating, which employs heat diffusion across the vessel walls into the growth solution, the microwave synthesis is more appealing as a green synthesis method because it can rapidly heat the entire volume of solution uniformly with precise control in temperature. Microwave-assisted synthesis has been recommended as one of the environmentally friendly methods by Patete.[15] Reaction rate, uniformity, selectivity, and energy saving of microwave assisted synthesis have been proven to be 1 order of magnitude higher than the water bath system. Katsuki et al. demonstrated that the conventional heating system consumed 6 times more energy than microwave heating in the synthesis of cubic $BaTiO_3$ nanoparticles.[16] Idalia et al. explained how microwave irradiation accelerated ZnO nanoparticle formation using zinc acetate and benzyl alcohol solution compared to conventional

Received: December 2, 2014
Accepted: February 4, 2015
Published: February 4, 2015

DOI: 10.1021/am508426z
ACS Appl. Mater. Interfaces 2015, 7, 4737−4743

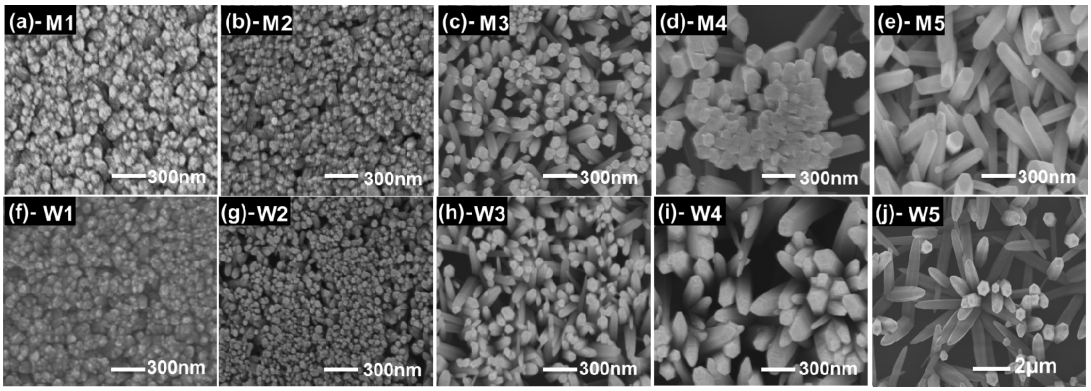

Figure 1. Top-view SEM images of the as-grown ZnO nanorods synthesized by (a−e) microwave (samples M1−M5) and (f−j) water bath (samples W1−W5) assisted solution methods at 90 °C for 20 min with 0.02 M $ZnAc_2$ and different [NH_3] (0.255 M, 0.503 M, 0.748 M, 0.988 M and 1.222 M).

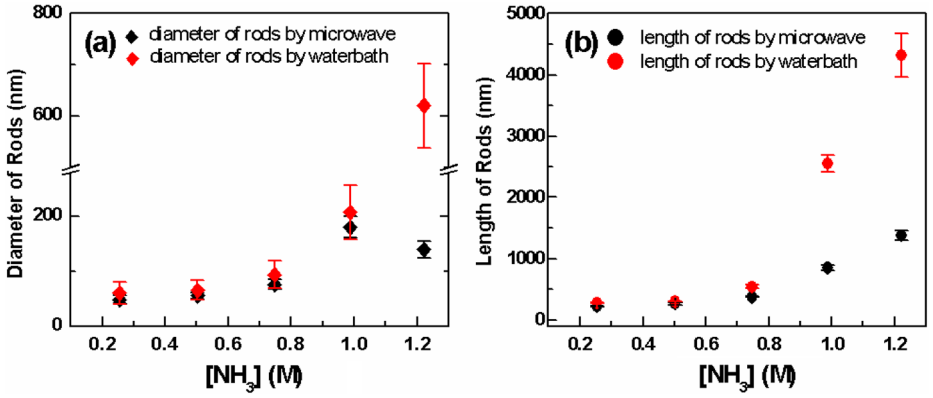

Figure 2. Statistical analyses of the (a) diameter and (b) length of the ZnO nanorods grown by microwave (samples M1−M5) and water bath (samples W1−W5).

heating from kinetic and thermodynamic aspects.[17] Richardson et al. also found that the increase in nucleation and growth rate of the epitaxial ZnO films on spinel was attributed to the fast heating rate of microwave assisted growth based on the classical nucleation theory.[18]

A general concern for the microwave synthesis is whether its attractive advantages come with a penalty in the crystal quality of the synthesized material. However, an accurate and systematic comparison on the defect and optical quality of ZnO nanostructures synthesized by both methods has yet been reported, which is highly desirable and will benefit the rapid production of fascinating ZnO devices.

In this study, we present a comprehensive and systematic study on the fundamental differences in the morphology, lattice structure, and optical properties of ZnO nanorods grown using the water bath and microwave heating routes. Our results show that under the same growth conditions, the main defect contributor for both microwave- and water-bath-grown samples are oxygen interstitials and zinc vacancies. However, microwave-assisted growth has fewer defects for both oxygen interstitials and zinc vacancies at the pH range of 10.5−10.9. After annealing, the defect levels for both methods were reduced but saturated to the same level. Therefore, for applications that can sustain high-temperature treatment, both methods are applicable in terms of crystal quality and defects, but microwave synthesis is faster and energy saving. For applications that cannot go through high-temperature treatment such as on plastic, paper, polymer, or other organic material substrates, microwave synthesis is recommended[19−22] because it is not only fast, energy saving, and uniform, but it also offers a better crystal quality for device performance, especially for band-edge transition optoelectronic devices.

2. EXPERIMENTAL PROCEDURE

In this experiment, the ZnO nanorods were grown on Si (100) substrates using two different aqueous solution routes: microwave and heated water bath. First, the bare Si (100) substrates were cleaned with acetone, isopropyl alcohol, and deionized (DI) water, followed by spin-coating of a ZnO seed layer[23] and rapid thermal annealing (RTA) for 5 min in air at 800 °C. After that, the substrates were submersed facing downward into 20 mL of the stock aqueous synthesis solution, which consists of 0.02 M zinc acetate dihydrate ($ZnAc_2$) with varying concentrations aqueous ammonia (hereafter, ammonia concentration will be denoted as [NH_3]). The different [NH_3] used were 0.255, 0.503, 0.748, 0.988, and 1.222 M, corresponding to the pH values of 10.07, 10.46, 10.65, 10.79, and 10.9 of the initial solution, respectively. A stock ammonia (NH_3) solution was prepared for each concentration to ensure that the chemical composition of the growth solutions for microwave and heated water bath are same. Microwave growth was carried out using a single mode 2.45 GHz microwave reactor with forced air cooling at a power of 100 W, while heated water bath growth was performed using a standard heated water bath. In both methods, the growth temperature was kept at 90 °C, and the growth duration was 20 min. After growth, the samples were cooled to room temperature naturally, rinsed thoroughly in DI water, and blown dry with nitrogen gas.

The morphologies of samples were characterized by field emission scanning electron microscopy (FESEM). The growth orientations of

DOI: 10.1021/am508426z
ACS Appl. Mater. Interfaces 2015, 7, 4737−4743

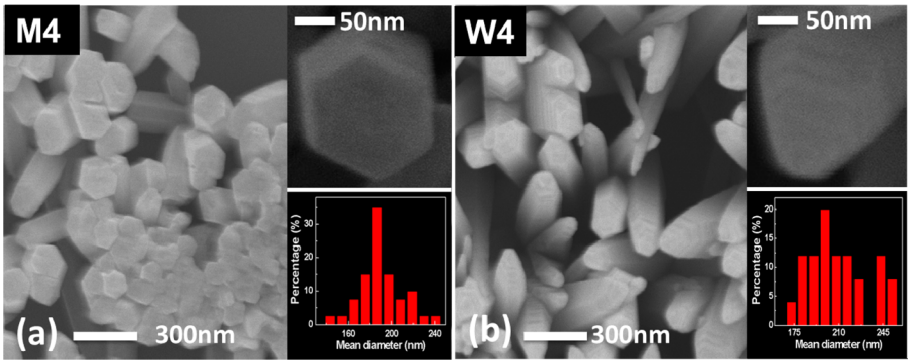

Figure 3. Top view of the ZnO nanorods grown with (a) microwave synthesis (M4) and (b) heated water bath (W4). (insets, top) High-magnification images of the tip of the nanorods and (insets, bottom) statistics of the nanorods diameter for samples M4 and W4.

the samples were analyzed using X-ray diffraction (XRD) by a general-area-detector diffraction system with a Cu Kα X-ray source.[24] X-ray photoelectron spectrometry (XPS) measurements were performed on the as-grown and annealed samples with monochromatic aluminum Kα (1486.6 eV) as excitation source. The annealing took place in the XPS chamber under high-vacuum conditions ($<1 \times 10^{-8}$ Torr) at 500 °C for 10 min. All XPS spectra were calibrated to the C 1s binding energy at 285.0 eV. Quantification of Zn to O ratios from the XPS survey spectra was performed with Thermo Advantage software and a Shirley background subtraction using the O 1s and Zn 2p3 peaks with relative sensitivity factors of 0.66 and 4.8, respectively.[25] Low-temperature photoluminescence (LTPL) measurements were performed at 20 K using a micro-PL system equipped with a closed-cycle He cryostat and a 325 nm He−Cd laser excitation source. Ultraviolet Raman scattering was carried out in a backscattering geometry at room temperature using a micro-Raman system with a 325 nm He−Cd laser. The laser was kept at a low power to avoid the thermal-induced redshift of the optical phonons.

3. RESULTS AND DISCUSSION

Top-view SEM images of the as-grown ZnO nanorods synthesized by both microwave and heated water bath methods at different $[NH_3]$ are shown in Figure 1. To measure the length of the ZnO nanorods, we also took side-view SEM images, which are shown in Figure S1 (Supporting Information). Statistical analyses of the diameter and length of the nanorods grown at each condition are plotted in Figure 2. It is observed that with the increase of $[NH_3]$ from 0.255 to 1.222 M, the nanorods become sparser and longer with larger diameters for both growth methods. Particularly, under higher $[NH_3]$, the diameters and lengths of microwave-synthesized M4 and M5 are significantly smaller than the corresponding W4 and W5 grown in heated water bath. Additionally, the nanorods in M4 and M5 have a flat end, while the ends of nanorods in W4 and W5 are tapered. Magnified views and detailed statistical analyses are shown in Figure 3.

Under the five different $[NH_3]$ used, the pH of the growth solution is in the range of 10.07−10.9, which is larger than the known point of zero charge (PZC) of ZnO.[18,26] In this growth regime, H_2O molecules adsorbed at the ZnO surface readily hydrolyze to release H^+ into the OH^- rich environment, allowing the negatively charged major growth units $Zn(OH)_4^{2-}$ to be adsorbed onto the positively charged polar Zn face and leading to a fast anisotropic growth rate along the *c* axis of ZnO. The growth orientation of the ZnO nanorods by both water bath and microwave methods are proved to be *c*-axis preferred as shown in Figure S2 (Supporting Information). The higher the pH is, the stronger the attraction between the solution and H^+ ions is and faster the growth rate will be. It is also known that at higher pH, the solubility of Zn in the aqueous solution will increase, which will influence the growth rate, morphology, and type of native defects in the ZnO nanorods.[27] As a result of the increase in Zn solubility, the supersaturation degree of ZnO decreases, leading to a lower initial nucleation rate and fewer nucleation sites, which is visualized in Figure 1 as a lower areal density of the grown nanorods. At higher pH, as the reservoir of soluble Zn is larger and available nucleation sites are fewer, the synthesized nanorods are longer with larger diameter.

In general, solution-grown ZnO nanorods have tapered ends resulting from the faster growth rate along the *c* direction than other directions. The flatter ends of microwave-grown nanorods at higher pH can be explained by the dissolution process. In microwave synthesis, the growth proceeds at a much faster rate than that of heated water bath synthesis, leading samples M4 and M5 to undergo dissolution in the presence of high concentrations of OH^-. The following chemical reaction takes place in the solution, which leads to a simultaneous deposition and dissolution of ZnO:

$$Zn(NH_3)_4^{2+} + OH^- \underset{\Delta}{\leftrightarrow} ZnO + NH_3 + H_2O \quad (1)$$

In this reaction, the $Zn(NH_3)_4^{2+}$ ions react with OH^- to form ZnO, pushing the equilibrium in reaction 1 to the right-hand side at temperature above 75 °C. At the end-of-growth, the concentration of $Zn(NH_3)_4^{2+}$ is reduced, pulling the equilibrium in reaction 1 back toward the left and resulting in the dissolution of ZnO. Thus, the ends of the microwave synthesized nanorods become flat and the diameter of the nanorods are smaller than that of nanorods synthesized by heated water bath.[28] The result reveals that the microwave heating is able to achieve end-of-growth condition faster than conventional heated water bath method due to the fast growth rate. The difference is more obvious at higher $[NH_3]$.

The XPS survey spectra of samples M1−M5 and W1−W5 showed that the synthesized ZnO nanorods are of high purity, with only the presence of carbon impurity. A typical XPS survey spectrum is shown in Figure 4a. The integrated area under O 1s peak and Zn 2p peak for as-grown samples at different $[NH_3]$ are summarized in Figure 4b. In Figure 4c, the quantified percentages of O 1s in ZnO for both as-grown and annealed samples are calculated. For the as-grown samples, the percentage of O in the as-grown ZnO sample rises from ~65% to ~80% as the $[NH_3]$ increases from 0.255 to 1.222 M. The increasing O to Zn ratio with respect to $[NH_3]$ can be attributed to the increased concentration of oxygen interstitials (O_i) or zinc vacancies (V_{Zn}). As mentioned earlier, with higher

DOI: 10.1021/am508426z
ACS Appl. Mater. Interfaces 2015, 7, 4737−4743

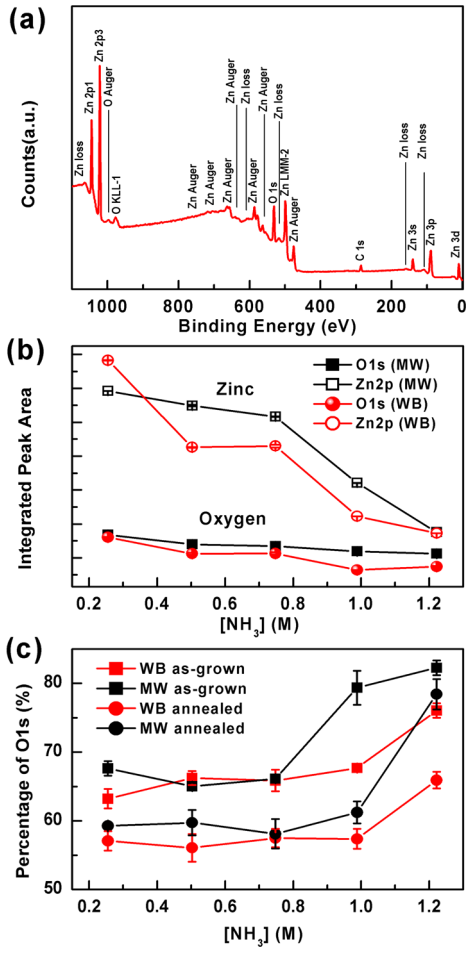

Figure 4. (a) Typical XPS survey spectrum of the ZnO nanorods. (b) Integrated area of O 1s and Zn 2p peaks for as-grown samples under different [NH_3]. (c) The quantified percentage of O 1s in ZnO of as-grown and annealed samples synthesized by heated water bath and microwave synthesis.

[NH_3], the higher growth rate will result in a faster dissociation of H^+ ions and provides more available sites for Zn^{2+} cations. In addition, at such higher growth rate, there is no sufficient time for Zn^{2+} to occupy every available site and excess hydroxyl groups to dehydrate. As a result, the lack of zinc and excess oxygen from the hydroxyl groups during the lattice formation lead to V_{zn} and O_i. Regarding the annealed samples, the O ratio is much lower compared to that of the as-grown samples and tends toward the stoichiometric 50%. It has been reported that migration barriers for V_{Zn} and O_i are 1.4 and 0.23−1.98 eV respectively, depending on the migration paths and defect charge states.[29,30] The presence of the migration paths with low migration barrier for both V_{Zn} and O_i intrinsic defects leads to the out-diffusion of O_i and V_{Zn} during the thermal annealing at 500 °C and thus the improved stoichiometric ratio.

A closer examination of the asymmetric O 1s peak shows that it can be deconvoluted into three Gaussian−Lorentzian components, as shown in Figure 5a, with sample M1 as an example. The lowest binding energy component, O1, centered at 529.9 eV is related to the O^{2-} ions in the ZnO lattice. The second component, O2, at 531.0 eV is assigned to O-related defects such as O_i. Finally, the third component, O3, at 532.3 eV is usually attributed to adsorbed water.[31−33] Figure 5b plots the ratio of O2 to the entire O 1s peak. It shows for both microwave and water bath grown samples the percentage of O2 peak increases with [NH_3], that is, there are more O_i defects at higher pH. This is in agreement with the results presented in Figure 4 and other reported results[27] that have explained the role of higher pH in accelerating the growth rate and incorporating more O-defects in an O-rich environment. Interestingly, Figure 5b also suggests that microwave results in a lower concentration of O-related defects, possibly due to the higher rotational kinetic energy provided, which leads to the reorientation of growth units. The dissolution occurred during microwave synthesis also helps to reduce the defects, as dissolution usually starts from defect sites that have high energy and are not stable.

When photoluminescence measurement conditions are kept constant, the ratio of visible to UV PL emission is a useful gauge to compare defect densities between different growth conditions. Figure 6a,b showed the LTPL spectra of as-grown samples by water bath and microwave, respectively, while Figure 6c,d presented the corresponding annealed samples. There are three peaks of interest: the UV band-edge at 3.37 eV (368 nm), the green emission at 2.55 eV (486 nm) due to V_{Zn},[34] and the orange emission at 2.04 eV (608 nm) due to O_i.[35] The dependence of the orange (green) to UV emission ratio on [NH_3] is plotted in Figure 7. The ratio of orange to UV emission increases with pH for both microwave- and water-bath-grown samples. In addition, the microwave synthesized ZnO has weaker orange emission compared to that of water bath synthesized ZnO, which means the density of O_i is lower. It is important to note that the green emission also increases

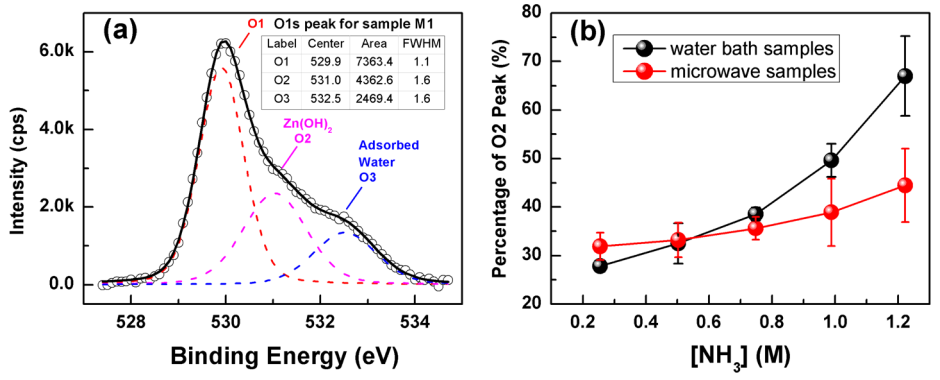

Figure 5. (a) XPS O 1s peak of sample M1 deconvoluted into three Gaussian−Lorentzian peaks (O1, O2, and O3, assigned in the plot). (b) Percentage of O2 in the total O 1s peak for as-grown samples.

DOI: 10.1021/am508426z
ACS Appl. Mater. Interfaces 2015, 7, 4737−4743

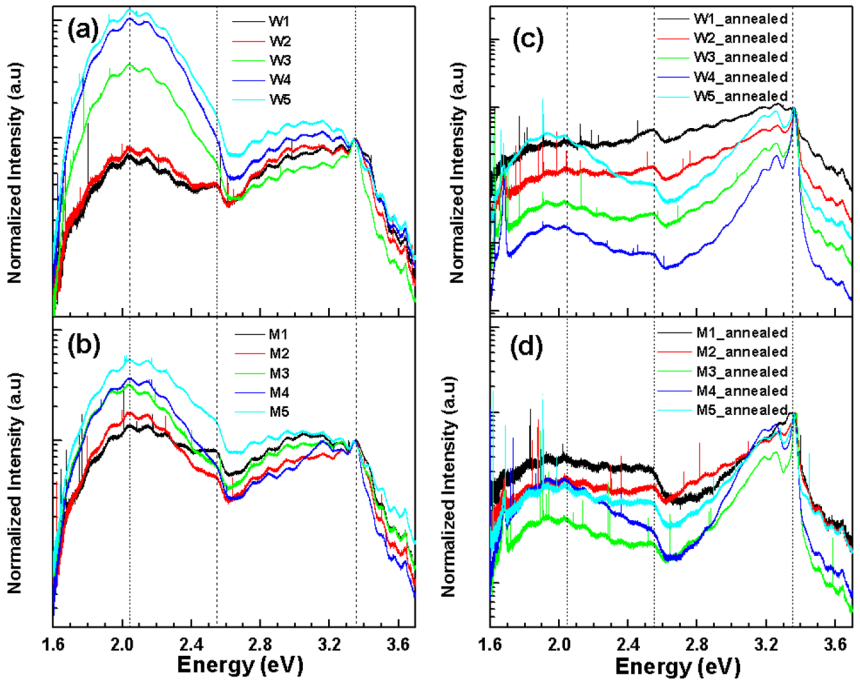

Figure 6. LTPL spectra of ZnO nanorods normalized to band-edge peak (3.37 eV) at 20 K for (a) as-grown water bath samples, (b) as-grown microwave samples, (c) annealed water bath samples, and (d) annealed microwave samples.

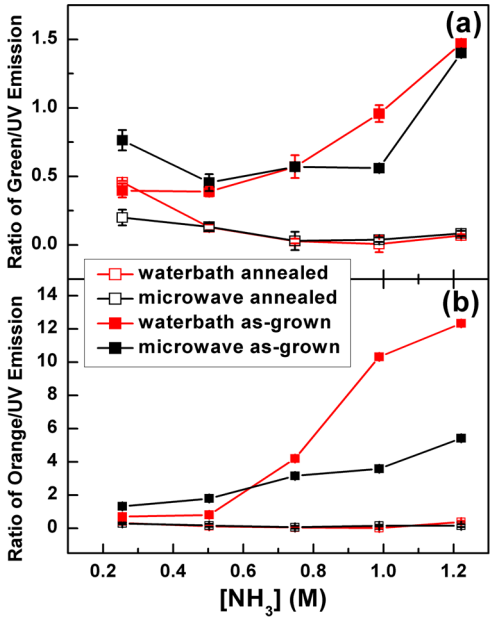

Figure 7. Ratio of (a) orange and (b) green emission to the band-edge emission for as-grown and annealed samples grown by both microwave and heated water bath.

with pH, suggesting that V_{Zn} is also the cause of the high O-to-Zn ratio. These results are in good agreement with the XPS data. After the samples are annealed, the ratios of orange and green to UV emission are reduced significantly, suggesting the out-diffusion of O_i and V_{Zn} and thus a more stoichiometric ratio of Zn to O, as seen earlier in Figure 4c.

The samples were further studied by UV Raman scattering. A typical result is shown in Figure 8a, where the Lorentzian peak fitting was employed to extract A_1(LO) phonon the—vibration of Zn−O bond along the *c* axis.[36] The peak at lower frequency is recognized as surface optical (SO) phonon mode which is caused by the columnar nature of the film.[37] As the absorption of 325 nm laser in ZnO is strong, the effect of the surface layer (a few monolayers) on Raman scattering is enhanced due to the Frohlich interaction.

A_1(LO) peak position of all the as-grown samples are plotted in Figure 8b. It is noticed that there is peak shift with respect to [NH_3]. The A_1(LO) frequency increases (blue shift) with the [NH_3] for both microwave synthesized and heated water bath samples, which is most possibly caused by the phonon localization of defects or impurities. Correlating with the oxygen and zinc defect analysis of the XPS O 1s and Zn 2p3 spectra, as well as the LTPL orange and blue emission peaks, it is apparent that the dominant mechanism for the shift in A_1(LO) peak is because of the presence of O_i and V_{Zn}. As O_i and V_{zn} both lead to a shorter Zn−O bond length, it results in larger compressive strain, and thus a blue shift of A_1(LO) peak frequency as [NH_3] increases.[36] This applies to both microwave and water bath grown ZnO samples. However, there is a discrepancy of ∼0.9 cm^{-1} between microwave and water bath samples. This is probably due to the faster growth rate with microwave synthesizer, which results in a larger compressive strain compared to those grown by heated water bath.

To make an in-depth comparison of the defects and crystal quality between microwave and water bath samples, we also examined the FWHM of the A_1(LO) peaks of the ZnO samples. A broader A_1(LO) line width implies poorer crystal quality, which is attributed to the intrinsic defects incorporated in the lattice.[37] As shown in Figure 9, the FWHM of the A_1(LO) phonon for microwave synthesized samples are smaller than those of the heated water bath samples with the same [NH_3], which indicates that the microwave-synthesized samples have fewer defects and better crystal quality as compared to the heated water bath samples grown using the same precursors.

DOI: 10.1021/am508426z
ACS Appl. Mater. Interfaces 2015, 7, 4737−4743

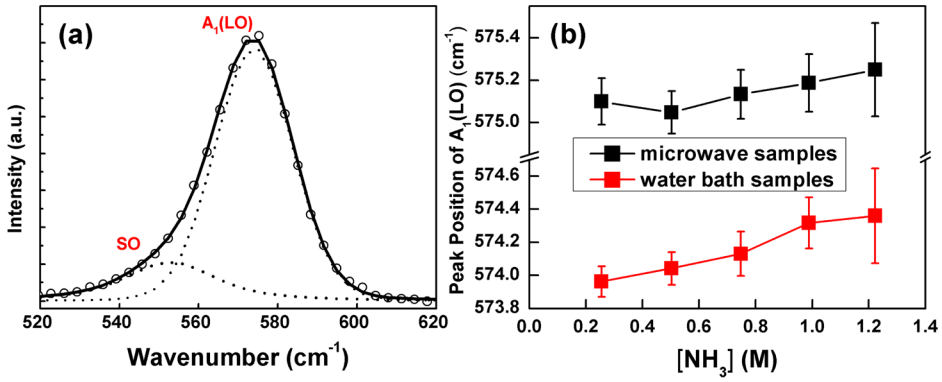

Figure 8. (a) The A_1(LO) and SO peak of Raman scattering for as-grown W1 measured at room temperature. (b) The measured A_1(LO) peak position for both microwave and heated water bath synthesized samples at different [NH_3].

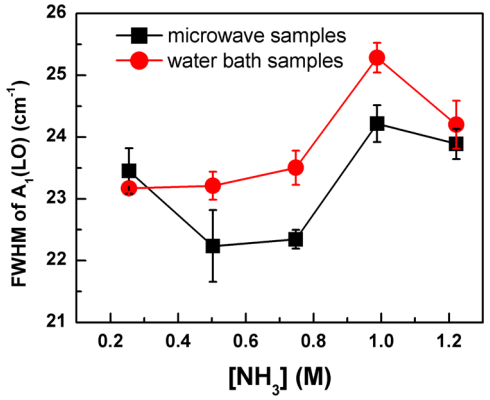

Figure 9. Fwhm of the A_1(LO) peak from Raman scattering measurement for the as-grown ZnO samples with different [NH_3].

4. CONCLUSIONS

A detailed comparative study on the differences between heated water bath and microwave synthesis methods for ZnO nanorods growth have been carried out. Compared to heated water bath, microwave synthesis has a faster growth rate with uniform size distribution of nanorods due to the unique ability to simultaneously heat the entire volume of solution. A benefit of the fast growth rate of microwave, the dissolution of ZnO nanorods also occurs within 20 min. As the dissolution starts with the defect sites that have higher energy, the defect level in microwave-grown ZnO is reduced. In addition, the rotational energy delivered by the 2.45 GHz microwaves allows the growth units to orientate themselves on the surface, leading to lower native defects such as O_i and V_{Zn}, which can be easily removed by postgrowth thermal annealing at 500 °C in vacuum. In summary, microwave synthesis presents a promising new approach in growing ZnO and other oxide nanostructures with low defect level and high bandedge emission compared to conventional water bath synthesis at low temperature, which is extremely attractive for the applications on low-cost, flexible substrates that cannot stand high temperature processes (e.g., plastic, paper, polymer, and organic materials). It also leads to new growth strategies for controlling the functionalities and morphologies of a wide range of metal oxide nanostructures by introducing rapid changes in temperature.

■ ASSOCIATED CONTENT

Supporting Information

Cross-sectional SEM images of the as-grown ZnO nanorods synthesized by microwave and water bath assisted solution methods at 90 °C for 20 min with 0.02 M $ZnAc_2$ and different [NH_3] (0.255 M, 0.503 M, 0.748 M, 0.988 and 1.222 M); XRD patterns collected from microwave and water bath grown samples. ZnO pattern: JCPDS 01-080-0075 is also shown in columns for comparison. This material is available free of charge via the Internet at http://pubs.acs.org.

■ AUTHOR INFORMATION

Corresponding Authors

*E-mail: elecsj@nus.edu.sg.
*E-mail: nnitcb@nus.edu.sg.

Notes

The authors declare no competing financial interest.

■ REFERENCES

(1) Feng, Z. C. *Handbook of Zinc Oxide and Related Materials. Volume 2, Devices and Nano-Engineering*; Taylor & Francis: Boca Raton, FL, 2012.
(2) Ozgur, U.; Hofstetter, D.; Morkoc, H. ZnO Devices and Applications: A Review of Current Status and Future Prospects. *Proc. IEEE* **2010**, *98*, 1255−1268.
(3) Djurišić, A. B.; Chen, X.; Leung, Y. H.; Ng, A. M. C. ZnO Nanostructures: Growth, Properties, and Applications. *J. Mater. Chem.* **2012**, *22*, 6526−6535.
(4) Perelshtein, I.; Applerot, G.; Perkas, N.; Wehrschetz-Sigl, E.; Hasmann, A.; Guebitz, G. M.; Gedanken, A. Antibacterial Properties of an In Situ Generated and Simultaneously Deposited Nanocrystalline ZnO on Fabrics. *ACS Appl. Mater. Interfaces* **2008**, *1*, 361−366.
(5) Park, S.-H.; Kim, S.-H.; Han, S.-W. Growth of Homoepitaxial ZnO Film on ZnO Nanorods and Light Emitting Diode Applications. *Nanotechnology* **2007**, *18*, 55608.
(6) Tang, J.; Deng, L. Y.; Tay, C. B.; Zhang, X. H.; Chai, J. W.; Qin, H.; Liu, H. W.; Venkatesan, T.; Chua, S. J. Determination of Carrier Concentration Dependent Electron Effective Mass and Scattering Time of n-ZnO Thin Film by Terahertz Time Domain Spectroscopy. *J. Appl. Phys.* **2014**, *115*, 33111.
(7) Izyumskaya, N.; Avrutin, V.; Schoch, W.; El-Shaer, A.; Reuss, F.; Gruber, T.; Waag, A. Molecular Beam Epitaxy of High-Quality ZnO Using Hydrogen Peroxide as an Oxidant. *J. Cryst. Growth* **2004**, *269*, 356−361.
(8) Qiu, J. H.; Guo, M.; Wang, X. D. Electrodeposition of Hierarchical ZnO Nanorod-Nanosheet Structures and Their Applications in Dye-Sensitized Solar Cells. *ACS Appl. Mater. Interfaces* **2011**, *3*, 2358−2367.

DOI: 10.1021/am508426z
ACS Appl. Mater. Interfaces 2015, 7, 4737−4743

(9) Nguyen, X. S.; Tay, C. B.; Fitzgerald, E. A.; Chua, S. J. ZnO Coaxial Nanorod Homojunction UV Light-Emitting Diodes Prepared by Aqueous Solution Method. *Small* **2012**, *8*, 1204−1208.
(10) Gao, P.; Chen, Y.; Wang, Y.; Zhang, Q.; Li, X.; Hu, M. A Simple Recycling and Reuse Hydrothermal Route to ZnO Nanorod Arrays, Nanoribbon Bundles, Nanosheets, Nanocubes, and Nanoparticles. *Chem. Commun.* **2009**, *19*, 2762−2764.
(11) Bao, D.; Gao, P.; Wang, L. Q.; Wang, Y.; Chen, Y. J.; Chen, G. R.; Li, G. B.; Chang, C.; Qin, W. ZnO Nanorod Arrays and Hollow Spheres Through a Facile Room-Temperature Solution Route and Their Enhanced Ethanol Gas-Sensing Properties. *ChemPlusChem.* **2013**, *78*, 1266−1272.
(12) Govender, K.; Boyle, D. S.; O'Brien, P.; Binks, D.; West, D.; Coleman, D. Room-Temperature Lasing Observed from ZnO Nanocolumns Grown by Aqueous Solution Deposition. *Adv. Mater.* **2002**, *14*, 1221−1224.
(13) Mahpeykar, S. M.; Koohsorkhi, J.; Ghafoori-Fard, H. Ultra-Fast Microwave-Assisted Hydrothermal Synthesis of Long Vertically Aligned ZnO Nanowires for Dye-Sensitized Solar Cell Application. *Nanotechnology* **2012**, *23*, 165602.
(14) Liu, N.; Fang, G.; Zeng, W.; Long, H.; Yuan, L.; Zhao, X. Novel ZnO Nanorod Flexible Strain Sensor and Strain Driving Transistor with an Ultrahigh 10^7 Scale "On"−"Off" Ratio Fabricated by a Single-Step Hydrothermal Reaction. *J. Phys. Chem. C* **2011**, *115*, 570−575.
(15) Patete, J. M.; Peng, X.; Koenigsmann, C.; Xu, Y.; Karn, B.; Wong, S. S. Viable Methodologies for the Synthesis of High-Quality Nanostructures. *Green Chem.* **2011**, *13*, 482−519.
(16) Katsuki, H.; Furuta, S.; Komarneni, S. Semi-Continuous and Fast Synthesis of Nanophase Cubic $BaTiO_3$ Using a Single-Mode Home-Built Microwave Reactor. *Mater. Lett.* **2012**, *83*, 8−10.
(17) Bilecka, I.; Elser, P.; Niederberger, M. Kinetic and Thermodynamic Aspects in the Microwave-Assisted Synthesis of ZnO Nanoparticles in Benzyl Alcohol. *ACS Nano* **2009**, *3*, 467−477.
(18) Richardson, J. J.; Lange, F. F. Rapid Synthesis of Epitaxial ZnO Films from Aqueous Solution Using Microwave Heating. *J. Mater. Chem.* **2011**, *21*, 1859.
(19) Xu, S.; Wang, Z. L. One-Dimensional ZnO Nanostructures: Solution Growth and Functional Properties. *Nano Res.* **2011**, *4*, 1013−1098.
(20) Manekkathodi, A.; Lu, M.-Y.; Wang, C. W.; Chen, L.-J. Direct Growth of Aligned Zinc Oxide Nanorods on Paper Substrates for Low-Cost Flexible Electronics. *Adv. Mater.* **2010**, *22*, 4059−4063.
(21) Costa, S. V.; Gonçalves, A. S.; Zaguete, M. A.; Mazon, T.; Nogueira, A. F. ZnO Nanostructures Directly Grown on Paper and Bacterial Cellulose Substrates without Any Surface Modification Layer. *Chem. Commun. (Camb).* **2013**, *49*, 8096−8098.
(22) Zhang, S.; Shen, Y.; Fang, H.; Xu, S.; Song, J.; Wang, Z. L. Growth and Replication of Ordered ZnO Nanowire Arrays on General Flexible Substrates. *J. Mater. Chem.* **2010**, *20*, 10606−10610.
(23) Zhao, Q.; Xu, X. Y.; Song, X. F.; Zhang, X. Z.; Yu, D. P.; Li, C. P.; Guo, L. Enhanced Field Emission from ZnO Nanorods via Thermal Annealing in Oxygen. *Appl. Phys. Lett.* **2006**, *88*, 33102.
(24) Liu, H. F.; Lim, E. S.; Tung, P. K. H.; Xiang, N. Fabrication and Transfer of Nanoporous Alumina Thin Films for Templating Applications: Metal Dots Array Deposition and Porous ZnO Film Growth. *Thin Solid Films* **2011**, *519*, 3050−3054.
(25) Briggs, D.; Seah, P. *Practical Surface Analysis: By Auger and X-Ray Photoelectron Spectroscopy*; Wiley: New York, 1990.
(26) Bilecka, I.; Elser, P.; Niederberger, M. Kinetic and Thermodynamic Aspects in the Microwave-Assisted Synthesis of ZnO Nanoparticles in Benzyl Alcohol. *ACS Nano* **2009**, *3*, 467−477.
(27) Tay, C. B.; Chua, S. J.; Loh, K. P. Investigation of Morphology and Photoluminescence of Hydrothermally Grown ZnO Nanorods on Substrates Pre-Coated with ZnO Nanoparticles. *J. Cryst. Growth* **2009**, *311*, 1278−1284.
(28) Wei, A.; Sun, X. W.; Xu, C. X.; Dong, Z. L.; Yang, Y.; Tan, S. T.; Huang, W. Growth Mechanism of Tubular ZnO Formed in Aqueous Solution. *Nanotechnology* **2006**, *17*, 1740−1744.
(29) Erhart, P.; Albe, K. First-Principles Study of Migration Mechanisms and Diffusion of Oxygen in Zinc Oxide. *Phys. Rev. B* **2006**, *73*, 115207.
(30) Erhart, P.; Albe, K. Diffusion of Zinc Vacancies and Interstitials in Zinc Oxide. *Appl. Phys. Lett.* **2006**, *88*, 201918.
(31) Bang, S.; Lee, S.; Ko, Y.; Park, J.; Shin, S.; Seo, H.; Jeon, H. Photocurrent Detection of Chemically Tuned Hierarchical ZnO Nanostructures Grown on Seed Layers Formed by Atomic Layer Deposition. *Nanoscale Res. Lett.* **2012**, *7*, 1−11.
(32) Jiang, S.; Ren, Z.; Gong, S.; Yin, S.; Yu, Y.; Li, X.; Xu, G.; Shen, G.; Han, G. Tunable Photoluminescence Properties of Well-Aligned ZnO Nanorod Array by Oxygen Plasma Post-Treatment. *Appl. Surf. Sci.* **2014**, *289*, 252−256.
(33) Hsieh, P.-T.; Chen, Y.-C.; Kao, K.-S.; Wang, C.-M. Luminescence Mechanism of ZnO Thin Film Investigated by XPS Measurement. *Appl. Phys. A: Mater. Sci. Process.* **2008**, *90*, 317−321.
(34) Janotti, A.; Van de Walle, C. G. Native Point Defects in ZnO. *Phys. Rev. B* **2007**, *76*, 165202.
(35) Li, D.; Leung, Y. H.; Djurišić, A. B.; Liu, Z. T.; Xie, M. H.; Shi, S. L.; Xu, S. J.; Chan, W. K. Different Origins of Visible Luminescence in ZnO Nanostructures Fabricated by the Chemical and Evaporation Methods. *Appl. Phys. Lett.* **2004**, *85*, 1601−1603.
(36) Irmer, G. Raman Scattering of Nanoporous Semiconductors. *J. Raman Spectrosc.* **2007**, *38*, 634−646.
(37) Schreder, B.; Kiefer, W. Raman Spectroscopy on II−VI−Semiconductor Nanostructures. In *Handbook of Raman Spectroscopy: From the Research Laboratory to the Process Line*; Lewis, I. R.; Edwards, H., Eds.; Marcel Dekker: New York, 2001; pp 491−548.

DOI: 10.1021/am508426z
ACS Appl. Mater. Interfaces 2015, 7, 4737−4743